Engineering Bio-compatible Interfaces via Combinations of Oxide Films and Organic Self-Assembled Monolayers

Xiaobo Yuan, Nikolaus Wolf, Timm J. J. Hondrich, Pegah Shokoohimehr, Frano Milos, Manuel Glass, Dirk Mayer, Vanessa Maybeck, Michael Prömpers, Andreas Offenhäusser and Roger Wördenweber*

Institute of Complex Systems – Bioelectronics (ICS-8), Forschungszentrum Jülich, Jülich 52428, Germany

ABSTRACT: In this paper we demonstrate that cell adhesion and neuron maturation can be guided by patterned oxide surfaces functionalized with organic molecular layers. It is shown that the difference in the surface potential of various oxides (SiO_2, Ta_2O_5, TiO_2, and Al_2O_3) can be increased by functionalization with a silane, (3-aminopropyl)-triethoxysilane (APTES), which is deposited from the gas-phase on the oxide. Furthermore, it seems that only physisorbed layers (no chemical binding) can be achieved for some oxides (Ta_2O_5 and TiO_2), whereas self-assembled monolayers (SAM) form on other oxides (SiO_2 and Al_2O_3). This does not only alter the surface potential, but also affects the neuronal cell growth. The already high cell density on SiO_2 is increased further by the chemically bound APTES SAM, whereas the already low cell density on Ta_2O_5 is even further reduced by the physisorbed APTES layer. As a result the cell density is ~8 times greater on SiO_2 compared to Ta_2O_5, both coated with APTES. Furthermore, neurons form the typical networks on SiO_2, whereas they tend to cluster to form neurospheres on Ta_2O_5. Using lithographically patterned Ta_2O_5 layers on SiO_2 substrates functionalized with APTES, the guided growth can be transferred to complex patterns. Cell cultures and molecular layers can easily be removed and the cell experiment can be repeated after functionalization of the patterned oxide surface with APTES. Thus, the combination of APTES-functionalized patterned oxides might offer a promising way of achieving guided neuronal growth on robust and re-usable substrates.

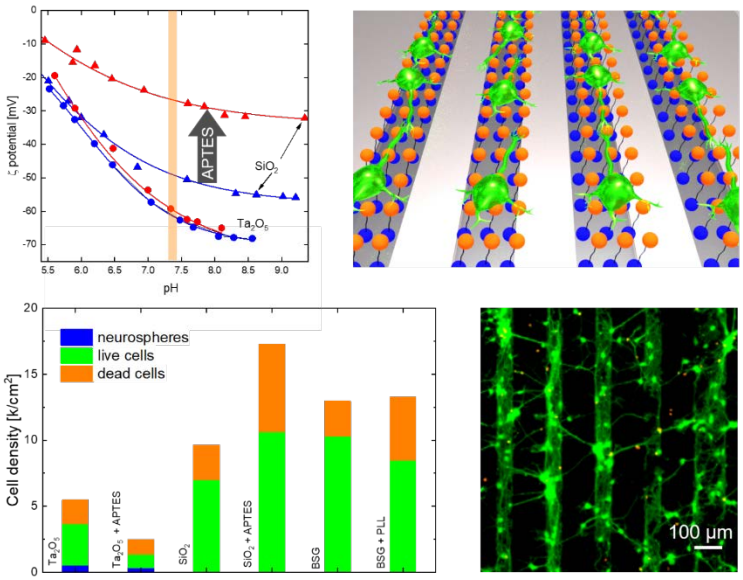

KEYWORDS: self-assembled monolayer, APTES, guided cell growth, patterned oxides, neuronal patterns, designed neuronal networks

INTRODUCTION

The ability to generate neuronal networks with constrained synaptic connectivity represents a promising approach to, on the one hand, studying the development and activity of small neuronal assemblies and, on the other hand, understanding and improving the interface between a typically abiotic substrate (including optional electronic components) and neurons. Both aspects are important for various bioelectronics applications ranging from neuronal cell-based sensors and actuators to neuronal logic devices [1-5]. The necessary directed growth of neuronal networks is usually obtained by confining the neurons (soma location and neurite elongation) to a predefined pattern.

This guided cell growth can be achieved either by directly positioning neurons on the substrate [6-10] or by functionalizing the substrate's surface in a way that leads to a preferential cell growth [11-18]. In the latter case, soft-lithography methods (for instance nano- or microcontact printing) represent the most commonly used technologies to functionalize the surfaces in a patterned way [4, 19-25]. As a result, cells show a preference for growth on either the functionalized or non-functionalized areas (depending on the functionalization). Candidates for the functionalization range from simple layers of organic molecules or proteins to self-assembled monolayers (SAM) [26-33]. Combinations are also possible [34-36]. SAMs especially provide versatile strategies to generate biofunctional surfaces. They are ultrathin (monolayer) and, due to their chemical binding to the substrate, quite robust [3]. Since they allow the physical and chemical properties of the substrate surface to be tailored in many ways, SAMs in combination with soft-lithographical methods are often used nowadays for guided cell experiments [37]. In order to achieve a large cells adhesion contrast, normally a backfill chemistry is need to block the unwanted docking sites for cells. Examples are polyethyleneoxy (PEG), octyltrichlorosilane (OTS), or lubricant-infused omniphobic coatings which attenuate non-specific adhesion of cells [38-39].

In this paper, the guided growth of neurons is achieved without any blocking material but using patterned SiO_2-Ta_2O_5 oxide surfaces, which are functionalized with organic molecules. The difference in the surface potential of the different oxides (SiO_2 and Ta_2O_5) themselves is already very large. This difference is strongly increased after functionalization of the oxides. Moreover, only physisorbed layers (no chemical binding) are achieved on Ta_2O_5, whereas covalently bound SAMs form on SiO_2. The different surface properties and molecular layer formations on the oxides strongly affect the neuronal cell growth (cell density and morphology). As a result we obtain robust and reusable substrates that show guided neuronal cell growth.

EXPERIMENTAL SECTION

Molecules: The silane 3-aminopropyltriethoxysilane (APTES, 99%) was obtained from Sigma-Aldrich (St. Louis). For the deposition, APTES was filled into a vacuum-tight glass flask, which was then connected via a valve to the deposition chamber.

Substrates: In this study, p-doped (111)-oriented silicon (Si-Mat, 3.6-6.5 Ω·cm) with a 90 nm-thick SiO_2- termination layer and a size of 10 mm×10 mm was employed for the investigation of

the selective self-assembled molecule deposition and cell growth. Furthermore, borosilicate glass (BSG) from Sigma-Aldrich (St. Louis) was used for cell growth reference.

Oxide films: Titanium oxide (TiO_2), aluminum oxide (Al_2O_3), and tantalum pentoxide (Ta_2O_5) films with a typical thickness of 30 nm were deposited on the 90 nm-thick SiO_2 by atomic layer deposition (ALD) (FlexAl, Oxford Plasma Technology). The precursors (from company Sigma-Aldrich; St. Louis) and substrate temperatures for the different oxides are: tetrakis(dimethylamino)titanium and 200 °C for TiO_2, trimethylaluminum and 130 °C for Al_2O_3, and tris(diethylamido)(tert-butylimido)tantalum(V) and 300 °C for Ta_2O_5. For the deposition standard recipes of Oxford Instruments Plasma Technology are used, an example of the resulting film properties is given in *Supplemental information Figure S1*.

Patterning: The patterning of the oxide films (here mainly Ta_2O_5 films) consists of two steps, the lithography and the etching.

Electron Beam Lithography: The oxide layer was coated with a photoresist (PMMA AR-P 669.07) via spin-coating at 4000 rpm for 60 s and subsequent baking at 120 °C for 30 min, resulting in a resist thickness of approximately 700 nm. In order to enhance the conductivity of the PMMA, a 10 nm Cr layer is deposited on the PMMA. The lithography is then performed via e-beam writing of the pattern (VISTEC EBPG 5000 plus). After e-beam writing, the Cr layer is etched away with a mixture of ceric ammonium nitrate, perchloric acid, and water. For the development of the PMMA, the sample is immersed in a developer (AR600-55) for 90 s.

Reactive Ion Etching (RIE): After the electron lithographic steps, the resulting pattern in the resist is etched into the Ta_2O_5 layer via reactive ion etching using a RIE device (Oxford Plasmalab 100). The parameters are a process gas mixture of O_2 and CF_4 (ratio 1:10) at a pressure of 0.004 hPa, a substrate temperature of ~20 °C, and a power of 10 W, yielding an etching rate of 0.6 nm/s. The remaining PMMA was removed in acetone in an ultrasonic bath for 15 min, then cleaned with propanol in an ultrasonic bath for 3 min, and dried with nitrogen gas. The resulting etching profile was checked with a Tencor Alphastep profilometer. A typical image of the resulting pattern is shown in Figure 1.

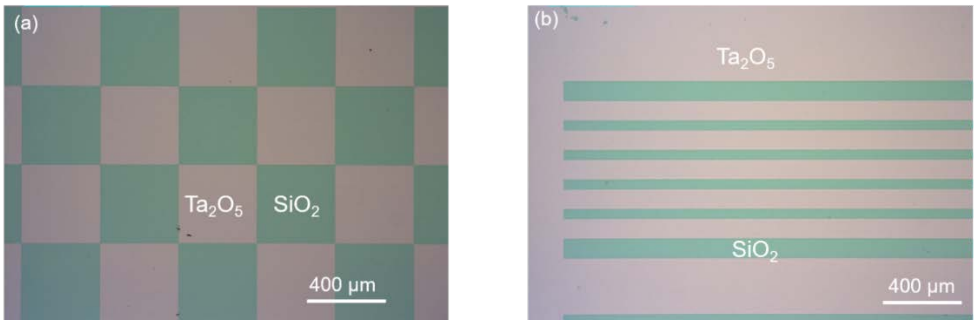

Figure 1. Microscope image of a patterned Ta_2O_5 layer on SiO_2 after e-beam lithography and RIE showing different test structures (chessboard (a) or bars (b)) consisting of Ta_2O_5 surfaces (reddish) and SiO_2 surfaces (greenish).

Cleaning process and activation: The cleaning and activation of the samples consist of two steps, the chemical cleaning followed by an ozone treatment (cleaning and activation).

Chemical cleaning: All substrates were first cleaned in a cleanroom environment in acetone (>99.9 %, Sigma-Aldrich) in an ultrasonic bath for 5 mins (25 °C at 320 W power and 37 kHz frequency) and subsequently in isopropyl alcohol (2-propanol, >99.8 %, Sigma-Aldrich) in an ultrasonic bath for 5 mins (the same parameters as above). The substrates were then dried in nitrogen gas flow.

Ozone cleaning: Since not all contaminations were removed from the substrate surface by the chemical cleaning step, we added a second cleaning step especially to remove organic residues from the surface. For this step, the substrates were placed in the molecular layer deposition (MLD) chamber, which was first evacuated to ~10^{-5} hPa and then flooded with oxygen (99.99 % purity; flow rate 93 sccm). Using downstream control, an oxygen pressure of 1 hPa was established and a microwave discharge (2.45 GHz, 700 W) was ignited, which led to the conversion of oxygen to ozone. The ozone was directed with the oxygen flow to the substrate and led to the removal of residual organic impurities and at the same time activated the oxide surface of the SiO_2-terminated Si or ALD oxides. Since the ozone treatment is performed in the MLD device (see section "Molecular layer deposition" below), the deposition of the molecular layer is done directly after the ozone treatment, i.e. on a freshly activated oxide surface. In all other cases, the state of activation of the surface has to be taken into account. This state changes back to the non-activated state after some time. This relaxation process depends on the type of oxides as shown in Figure 2.

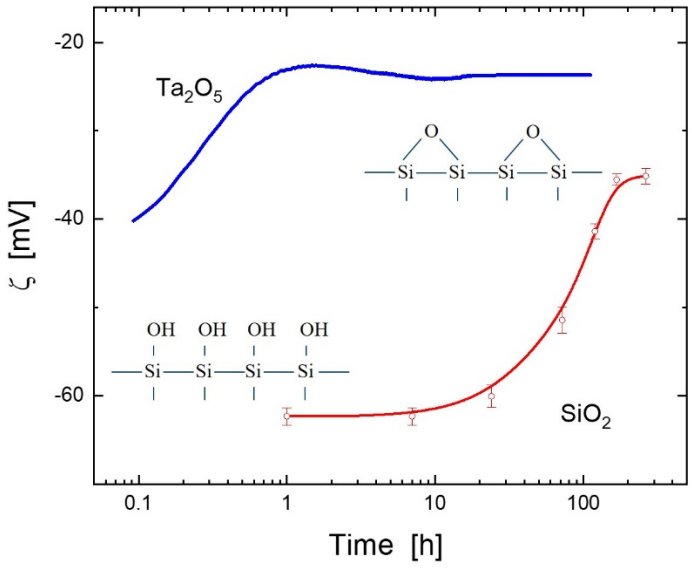

Figure 2. Time dependence of the ζ potential of SiO_2 and Ta_2O_5 measured in a 1 mM KCl electrolyte at pH 6.0 and pH 5.6 respectively. The schematics show the change of surface from the activated to the non-activated state for SiO_2.

Molecular layer deposition: APTES was deposited from the gas phase using a specially developed MLD device (see *Supplemental Information Figure S2*). It allowed us to perform all the important deposition steps including (i) surface activation using ozone, (ii) subsequent molecular deposition from the gas phase, and (iii) post-deposition treatment without breaking the vacuum. The different process steps are explained in detail in the references [40, 41].

Surface activation: The activation with ozone is identical to the ozone cleaning process described above. An exposure of the oxide surface to ozone for 3 mins was sufficient to obtain an activated SiO_2 surface, which was demonstrated, for instance, by the significantly reduced surface potential of ~ (-62 ± 1) mV (Figure 2) and a contact angle below 20^o.

Deposition process: After surface activation, the oxygen supply was turned off and the deposition process gas (Ar) switched on. We used an Ar flow of 27 sccm and established a process pressure of 0.1 hPa. The actual deposition of APTES was initiated by opening the valve of the molecule source. After 10 minutes of deposition, the valve of the molecule source was closed and the actual deposition terminated.

Post-deposition treatment: After the actual deposition, the samples were kept in the MLD device in a vacuum for 24 hours. This post-deposition treatment turned out to be vital for the formation of APTES SAMs prepared by room temperature gas phase deposition on SiO_2 (see *Supplemental Information Figure S3*) [40].

Streaming current measurements: The surface potential of the oxides and molecular layers was analyzed by a modified electrokinetic analyzer (SurPASS, Anton Paar Germany GmbH). A pair of identical planar substrates were placed in a clamping cell, with the surfaces that were being analyzed facing each other and forming a microfluidic channel with a gap size of typically ~75 μm (see *Supplemental Information Figure S4*). The ζ potential was determined using the Helmholtz–Smoluchowski equation,

$$\zeta = (dI/dp)(\eta L/\varepsilon\varepsilon_o A),$$

Where p is the pressure necessary to generate the laminar flow; η and ε are the viscosity and dielectric constant of the electrolyte; ε_o is the vacuum permittivity; L and A represent the length and cross section of the flow channel, respectively; and I is the resulting current measured between two electrodes placed at each side of the measuring cell. The resulting ζ potential represents the electrokinetic potential at the shear plane between the mobile and immobile Helmholtz layers and is a measure of the surface potential [42].

The pH value of the electrolyte is adjusted via titration. In this study, we focused on the pH range (pH 5-9) covering the physiological conditions, pH 6-8, for the natural milieu of organism and cell systems. Electrolyte and titration solutions are aqueous solutions based on ultrapure water (Milli-Q) containing potassium chloride (1 mM KCl) in the case of the working electrolyte and a gradual titration using a basic electrolyte of 50 mM KOH. During the experiment, the temperature of the medium was kept constant at 25 °C. Furthermore, the reservoirs for the working electrolyte and the titration electrolyte were encapsulated to minimize contact with air and a N_2 purger was used to suppress the formation of hydrocarbonates (HCO_3^-), which can form if CO_2 is dissolved in the

aqueous solution. Prior to each experiment, the experimental setup was rinsed with 2 L of ultrapure water and subsequently with the working electrolyte solution.

Fluorescence Microscopy: Fluorescence microscopy investigations of the molecular layers and cell cultures were carried out via a Zeiss Apotome microscope using the Zen software. Fluorescein isothiocyanate (FITC), a fluorescein molecule functionalized with an isothiocyanate reactive group replacing a hydrogen atom on the bottom ring of the structure, is used as an optical marker. It is reactive with respect to nucleophiles, including amine and sulfhydryl groups on proteins, and thus binds to APTES (the structure of FITC and its reaction mechanism is shown in Figure 3). FITC was mixed with ultrapure water to a concentration of 10 µg/mL. The samples were coated with a drop (45 µL) of the FITC solution and kept at room temperature for 1 h avoiding any exposure to light. The remaining drop including all unbound FITC was then removed from the surface by rinsing with ultrapure water for 5 min and purging in a N_2 flow. As a result, only FITC that is bonded to chemisorbed APTES remains on the surface, unbound FITC and FITC bonded to only physisorbed APTES is removed during the rinsing.

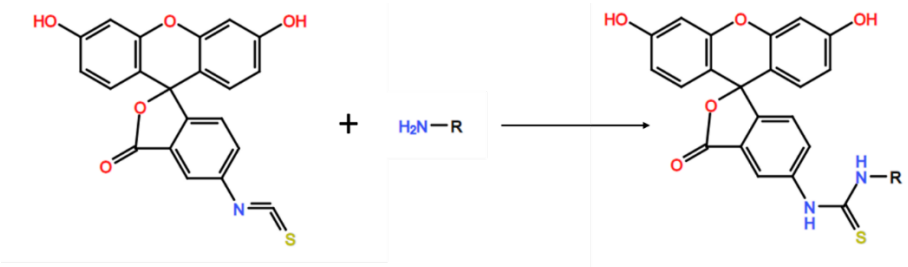

Figure 3. Schematic of the reaction of FITC with amine-containing compounds like APTES [43].

Neuronal Culture: Before preparation of the cell culture, the samples were sterilized by dipping them into ethanol for a few seconds and subsequently removing the ethanol in a N_2 flow. Cortical neurons were obtained from E18 Wistar rat embryos. Briefly, the cortex was dissected from the embryonic brain tissue and digested with trypsin-EDTA at 37 °C, 5 % CO_2, and 100 % humidity for 10 min. To remove trypsin, the cortex was washed three times with neurobasal medium (Life Technologies GmbH, Germany) supplemented with 1 % B27 (Life Technologies, Germany), 0.5 mM L-glutamine, and 50 µg/mL gentamicin. Then, the cortex was dissociated gently with a 1 mL pipette. Cell clumps and glia cells were allowed to settle for 2 min at room temperature. The supernatant was diluted in supplemented neurobasal medium, and 100 k cells per substrate per well were plated in a 12-well culture dish. The medium was replaced completely 4 h after plating. Over the following days, half of the medium was changed twice per week. Animal work was carried out with the approval of the Landesumweltamt für Natur, Umwelt und Verbraucherschutz Nordrhein-Westfalen, Recklinghausen, Germany, number 84-02.04.2015.A173.

Live/Dead Imaging: Live/dead staining was performed using 1 µg/mL calcein-AM and 2 µM ethidium homodimer (both Life Technologies) in supplemented cell growth medium to stain live

and dead cells green and red, respectively. Cells and dyes were incubated for 15 min at 37 °C. The live/dead image was typically conducted at DIV 6.

Critical point drying (CPD) and scanning electron microscopy (SEM): The substrate was rinsed 3 times with PBS (37 °C, Sigma Aldrich, USA), then fixed with diluted glutaraldehyde (Sigma Aldrich, USA) in PBS (3.2%) for 15 min at room temperature, followed by rinsing with PBS and with 2 L of ultrapure water to remove the fixative residues. Then, the water was exchanged via an ethanol series of 5 min in 10 %, 30 % and 50 %, 15 min in 70%, and 3 times for 5 min each in 90 % and 95 %. Then, the sample was stored in 100 % ethanol at 4 °C, and in a next step transferred into the chamber of the critical point drying (CPD) system (CPD 030, BAL-TEC Company), which was filled with 100 % ethanol. First, the chamber was slowly cooled down to 10 °C, and then ethanol was exchanged with liquid CO_2. This exchange process was repeated several times until the chamber was filled mainly with liquid CO_2. Then, the temperature of the chamber was increased up to 40 °C, followed by an increase in pressure to 73.8 bar causing the transformation of CO_2 into a supercritical form. Eventually, the chamber was evacuated, and the sample was dried and dehydrated.

The subsequent SEM characterization of the dried cell culture was carried out with a Gemini 1550 instrument (Leo/Zeiss) using an in-lens detector. To enhance conductivity, a thin layer of platinum (approximately 5 nm) was sputtered onto the sample. The imaging was taken at 1 kV acceleration voltage.

RESULTS AND DISCUSSION

The discussion of the results is divided into three sections. In the first part, we demonstrate that silanization with APTES is only possible for some of the oxides, whereas no APTES SAM forms on others. As a result we obtain a large difference in the surface potential as well as functionalization via APTES for the different oxides. In the second part we show that this difference leads to a large discrepancy in the compatibility with neuronal cell for these oxides. In the third part we demonstrate guided cell growth using patterned samples consisting of oxides of different biocompatibility.

I. Functionalization of different oxides with APTES

In this section, the surface potential of different oxides and their ability to be functionalized using APTES SAMs are discussed. Four candidates are examined, i.e. SiO_2 terminated Si, and Al_2O_3, TiO_2, and Ta_2O_5 films on Si. The ALD preparation of the films is described in the experimental section. In a first experiment we record the ζ potential of the different materials for the cleaned surface and for comparison after deposition of APTES (cleaning and APTES deposition are described in the experimental part). In order to demonstrate the presence or absence of APTES SAMs after APTES deposition, fluorescence microscopy experiments are performed for the different oxides.

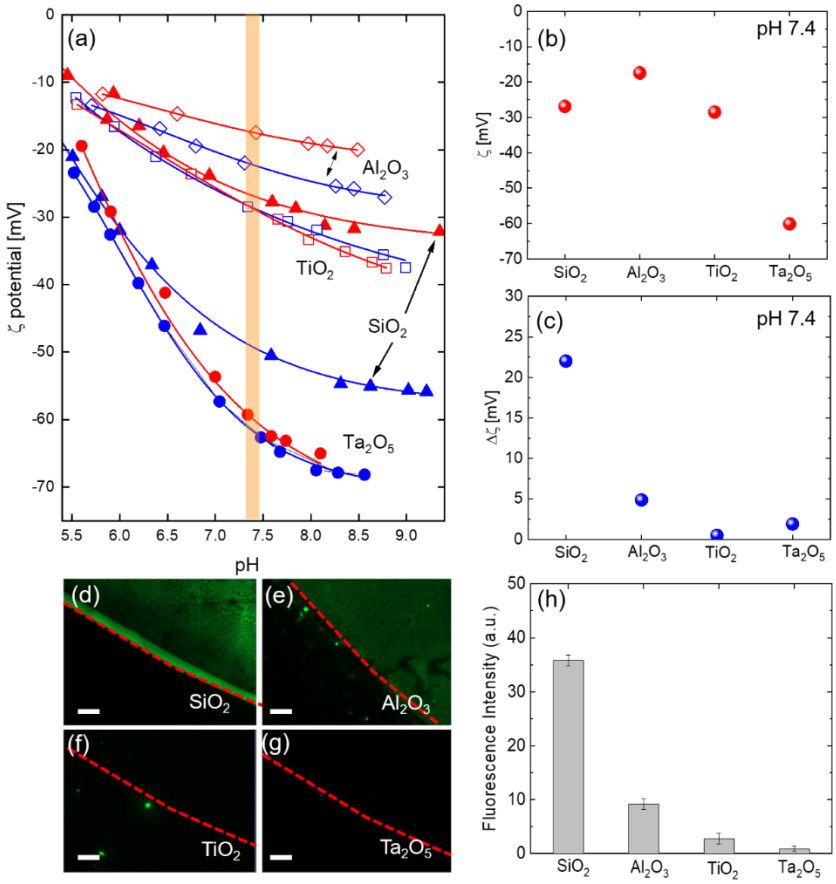

Figure 4. (a) ζ potential of TiO_2 (open squares), Al_2O_3 (open diamonds), Ta_2O_5 (solid circles), and Si/SiO_2 (solid triangles) in the cleaned state (blue) and coated with an APTES SAM (red), respectively, as a function of pH value for 1 mM KCl electrolyte. The orange shaded area depicts the physiological pH value of 7.4. (b), (c) represent the ζ potential (APTES coated) and Δζ (difference between the ζ potential for APTES coated and cleaned state) for the different oxide films at pH 7.4. (d), (e), (f), (g) present the fluorescence microscopic image of FITC drops on SiO_2, Al_2O_3, TiO_2 and Ta_2O_5 treated with APTES, respectively. The dashed red lines mark the boarder of the drop separating the FITC covered area (upper part) and the area without FITC (lower part); the scale bar is 100µm. (h) shows a comparison of the resulting FITC fluorescence intensities of APTES on the different oxides surfaces.

Figure 4a shows a set of titration experiments for the different oxides in the different states after cleaning and coating with APTES. In all cases, the titration measurement starts at pH ≈ 5.5 (1 mM KCl electrolyte), subsequently the pH value is increased incrementally with a basic (50 mM KOH) electrolyte. The titration experiments show the typical pH dependence of the ζ potential of oxides in the pH regime above the isoelectric point (i.e. the pH value of ζ = 0). The ζ potential decreases with increasing pH for all oxides and seems to saturate at high pH values (e.g. for SiO_2 and Ta_2O_5). However, there are two important differences between the different oxides:

(i) First, there is a significant difference in the height of the ζ potential for the different oxides. For example, at physiological conditions (pH ≈ 7.4), ζ potentials of around -22 mV and -62 mV are determined for Al_2O_3 and Ta_2O_5, respectively (see Figure 4b). This represents a large difference in the surface potential, which should also affect the cell adhesion property of the different oxides.

(ii) Second, for some oxides (SiO_2 and Al_2O_3) the APTES deposition leads to a clearly visible increase of the ζ potential, whereas for the others (TiO_2 and Ta_2O_5) no increase of the ζ potential is recorded. The largest increase is actually visible for SiO_2, where the ζ potential at physiological conditions changes from -49 mV to -27 mV (see Figure 4c). From previous work [40, 41] we know that the enhancement of the surface potential is an indication for the successful deposition of APTES, i.e. the formation of an APTES SAM on the oxide.

In order to demonstrate the presence of APTES SAMs on the oxides, fluorescence experiments were performed. By depositing a drop of FITC on each sample and removing the unbound FITC after some time (see experimental section), we can visualize the presence of APTES on the oxide, since FITC will only remain at APTES molecules bound to the sample. Figure 4d-4g show the edge of the drop for SiO_2, Al_2O_3, TiO_2 and Ta_2O_5. Whereas the fluorescence signal is clearly visible for SiO_2, no fluorescence can be observed for Ta_2O_5. Similar results are obtained for Al_2O_3 (fluorescence is visible) and TiO_2 (no fluorescence). This is summarized in Figure 4h. Since there is clear correlation between the FITC's fluorescence intensity and the amount of APTES on the oxides [41], this supports the result of the ζ potential measurement (compare Figures 4c and 4h) and leads to the conclusion that an APTES SAM formed on SiO_2 and Al_2O_3, but not on Ta_2O_5 and TiO_2.

The different properties of the oxides offer opportunities for the envisioned cell experiments. The large difference in the ζ potential, and the fact that one oxide can be functionalized with APTES and the other not, especially make SiO_2 and Ta_2O_5 promising candidates for comparative cell experiments.

II. Neuronal cell growth on SiO_2 and Ta_2O_5

In a second step, we analyze the neuronal cell growth on SiO_2 and Ta_2O_5 in the different states after cleaning and after APTES deposition. For comparison, BSG reference samples (only chemically cleaned; see experimental section) with and without poly-lysine (PLL) coating are added.

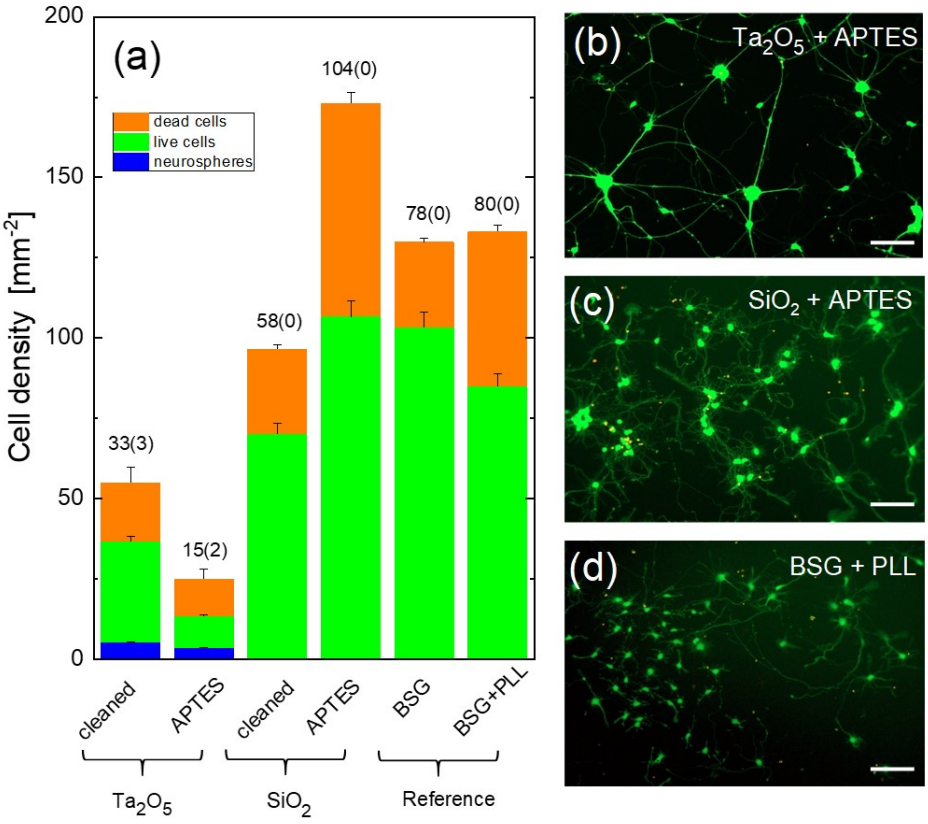

Figure 5. (a) Statistics of neurons after DIV 6 of incubation on Ta_2O_5 and Si/SiO_2 at different states (ozone cleaned and APTES-coated) and on BSG samples with and without PLL. The total number of live cells (green bars), dead cells (orange bars), and neurospheres (blue bars), the number of neurospheres (in brackets) obtained on average over several areas of size 0.6 mm^2 are added together to form the different columns; for the statistics 6 samples were investigated for each group. (b), (c) and (d) represent fluorescent microscope images of live/dead cell distributions for APTES modified Ta_2O_5 and SiO_2 and BSG treated with PLL, respectively; the scale bar is 100µm.

Figure 5 shows cortical neuron cells live/dead density obtained on Ta_2O_5, SiO_2, and the reference samples (BSG) for the different treatments, Figure 5b-5d show examples of fluorescence images obtained after live/dead staining (see experimental section), whereas in Figure 5a the statistics derived from these images (the results of 6 samples were always averaged for the statistics) are presented. The main results of this comparison are as follows:

(i) Whereas cell cultures on SiO_2 show live cell densities comparable to the reference samples (BSG with and without PLL), the neuron live density on Ta_2O_5 is significantly lower.

Moreover, neurons only tend to form clusters (neurospheres), which will be discussed below, on Ta_2O_5.

(ii) The impact of the APTES deposition on the cells' total density and cells' live density is opposite for SiO_2 and Ta_2O_5. For SiO_2, both densities (total and live density) increase after APTES deposition, whereas the densities decrease in the case of Ta_2O_5.

These observations demanded further discussion. First, from Figure 4 we know that APTES chemically binds to SiO_2 but not to Ta_2O_5. Nevertheless it is known that during the gas phase deposition, APTES is physisorbed on both oxide surfaces [40]. After deposition the physisorbed molecules will be desorbed. However this desorption process is a very slow process and can take hours. Therefore we encounter two different situations: in the case of the APTES deposition for SiO_2, we expect a layer of chemically bound APTES (SAM) and only a few physically bound molecules, whereas in the case of the Ta_2O_5, only physisorbed APTES is present (see *Supplemental Information Figure S3*), which can easily be removed from the surface. Therefore for SiO_2, the APTES SAM leads to a large increase of the surface potential and thus to a significantly higher total density of cells (i.e. actually close to the seeding cell density used for the preparation (see Figure 5a), whereas in the case of Ta_2O_5, the cells will adhere to a physisorbed layer of APTES and therefore can easily be removed from the Ta_2O_5 surface. Therefore, we have in one case (APTES chemisorbed SAM) an increase of the cell density and in the other case (physisorbed APTES) a decrease of the cell density.

With this explanation, we can also understand the first observation and especially the difference in the cell density shown in the Figure 5a. Neglecting the APTES-coated Ta_2O_5 where cells might be detached due to the physisorbed APTES coating, the surface potential seems to be correlated with the cell density. The total cell density (live and dead cells) is lowest for cleaned Ta_2O_5 (ζ (pH 7.4) $\approx$ -62 mV), higher for cleaned SiO_2 (ζ (pH 7.4) $\approx$ -49 mV), and highest for APTES-coated SiO_2 (ζ (pH 7.4) $\approx$ -27 mV). The higher the surface potential, the more cells seem to adhere.

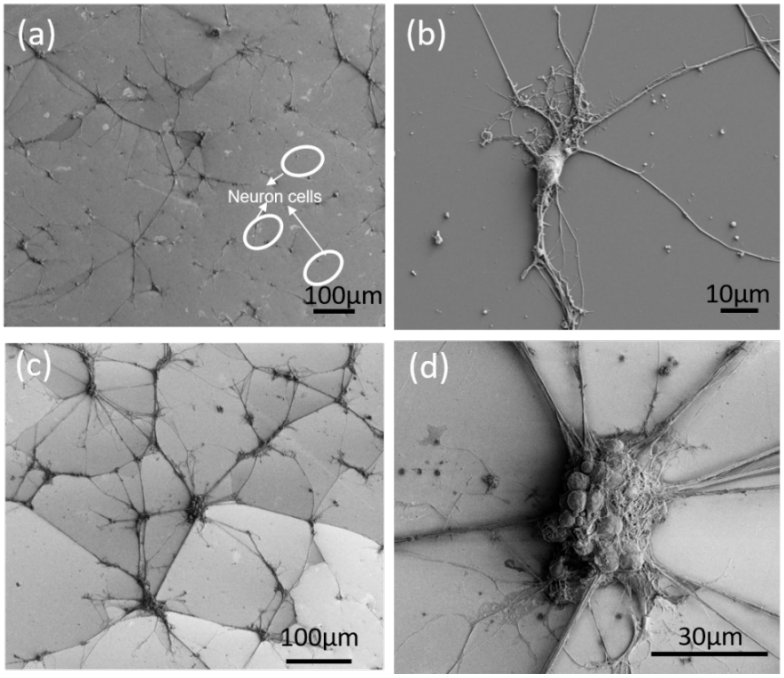

Figure 6. SEM morphology of CPD cortical neuronal cells with different magnification on APTES-coated SiO_2 (a), (b) and Ta_2O_5 (c), (d).

The formation of neurospheres might also be a result of the extremely negative surface potential of Ta_2O_5, since it is observed in the cases of both the cleaned and the APTES-coated Ta_2O_5. Figure 6 shows a comparison of neuron growth on SiO_2 and Ta_2O_5, both coated with APTES. Whereas healthy individual cells with extended neurites are observed on SiO_2, cells tend to form neurospheres of sizes up to 50 µm and tens of somas adhering together on Ta_2O_5. It even seems that most of these neurospheres are detached from the Ta_2O_5 and adhere to the top of individual dead cells. Even their axons and dendrites seem to form bundles with poor adhesion to the Ta_2O_5 surface, as indicated by lack of branching (see Figure 6d).

In conclusion to this section, we can state that a large contrast exists for the neuronal cell growth on SiO_2 and Ta_2O_5. Not only do cells tend to grow in neurospheres with poor adhesion to the surface on Ta_2O_5, whereas they grow individually on SiO_2, but there is also a large difference in the total cell density for cultures on these oxides. For cleaned substrates, there is a twofold difference in cell population on SiO_2 versus Ta_2O_5. By coating the oxides with APTES, this difference increases to eightfold. The higher the contrast, the more accurate substrate patterns are expected to be transferred to cell network geometries. Moreover, the density of living cells on APTES-coated SiO_2 is comparable and even slightly higher than that of reference samples prepared by standard cell culture, for instance on PLL-coated BSG. In the following section, the large difference in cell growth on APTES-coated SiO_2 and Ta_2O_5 surfaces is used to demonstrate guided cell growth.

III. Guided cell growth on patterned oxides

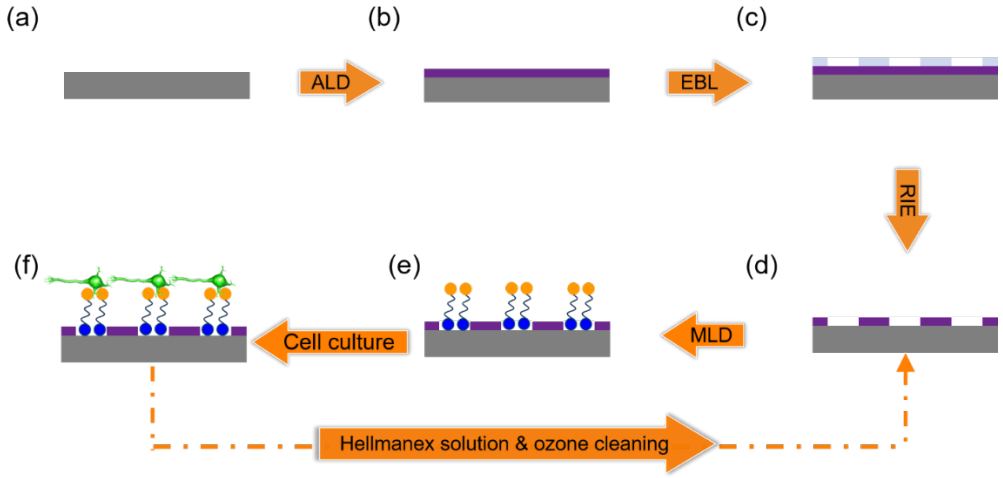

Figure 7. Schematic of substrate preparation process, MLD modification and cell culture for the guided neuron growth: (a) SiO_2-terminated Si substrate, (b) ALD of Ta_2O_5, (c) e-beam lithography, (d) reactive ion etching in order to partially remove the ALD layer, (e) MLD of APTES forming SAMs on SiO_2 surfaces and a physisorbed layer on Ta_2O_5, and (f) cortical neuron cell culture. After inspection and analysis, the cell culture can be removed with Hellmanex solution and after ozone-assisted removal of the remaining organic molecules, the process can be repeated starting with the MLD process (dashed-dotted line).

In the following we use the large cell density contrast of neuron growth on the APTES SAM-coated SiO_2 and Ta_2O_5 to achieve guided cell growth. The schematic in Figure 7 illustrates the different preparation steps (for detail see experimental section). The preparation of the patterned SiO_2-Ta_2O_5 oxide substrate starts with a 90 nm SiO_2 terminated Si substrate, which is coated with a 30 nm thick ALD Ta_2O_5 layer (Figure 7a and 7b). Using EBL and RIE, we generate the desired oxide pattern on the sample (see also Figure 1). As such, the sample represents a robust and reusable substrate for the subsequent deposition of molecules and cell culture. The deposition of APTES is done in the usual way (see experimental section) starting with an ozone activation of 3 min, followed by the actual gas phase deposition of the molecules (10 min, 0.1 hPa, vapor pressure) and finalized by a 24 h post-deposition treatment in a vacuum [40]. The neuron cell culture starts directly after the MLD preparation according to the procedure given in the experimental section, once again using a cell seeding concentration of approximately 28.6 k/cm^2.

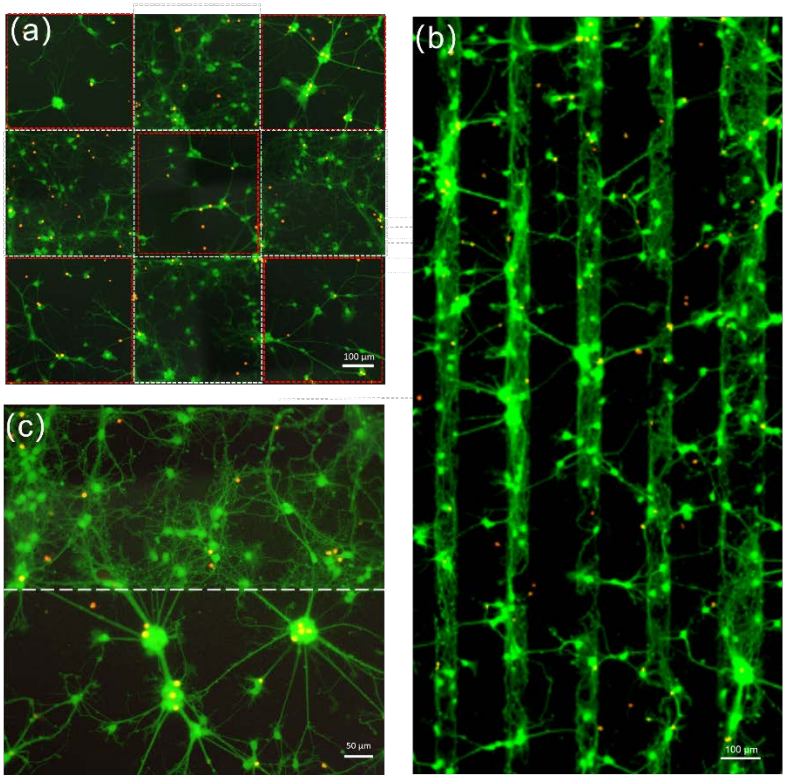

Figure 8. Fluorescent microscope images of cortical neuron cells on a patterned and APTES-coated Ta_2O_5-SiO_2 sample at DIV 6 of incubation showing guided cell growth: (a) cells form networks inside SiO_2 squares (white marked areas), whereas neurospheres are seen on Ta_2O_5 mainly inside Ta_2O_5 square (red marked areas), (b) regular neuron cell growths within the SiO_2 strips (50 µm and 100 µm-wide) separated by Ta_2O_5 (100 µm-wide) and (c) neuron networks in the area (above white dashed line) consisting of SiO_2 stripes (2 µm-wide) separated by Ta_2O_5 (1 µm-wide) and neuronspheres in the area of Ta_2O_5 (below white dashed line).

For this first test we chose three relatively simple structures:

(i) larger SiO_2 areas (400 µm × 400 µm squares) surrounded by Ta_2O_5 (see Figures 1a and 8a),
(ii) large SiO_2 strips (width of 50 µm or 100 µm) surrounded by Ta_2O_5 (see Figures 1b and 8b),
(iii) small SiO_2 strips (width of 2 µm) separated by 1 µm-wide stripes of Ta_2O_5 (see Figure 8c).

All patterns lead to a guided neuron growth behavior and show a growth morphology similar to that demonstrated in the previous section. Moreover the neuron cell culture can be repeatedly prepared according to the scheme shown in Figure 7 leading a reproducible guided growth behavior similar to those shown in the following Figures 8 and 9. On SiO_2 we observe a higher density of individual neurons, no neurospheres, and a high density of neurites, whereas a much lower density of neurons, mainly neurospheres, bundled axons and a low density of dendrites are present on Ta_2O_5 areas (see Figure 8). Interestingly, the third structure in Figure 8c, which consists of a series (137) of 2 µm-wide SiO_2 stripes disrupted by 1 µm Ta_2O_5, also behaves similarly to the plain SiO_2 areas in Figure 8a. It seems that the tiny Ta_2O_5 disruptions do not affect the neuron growth. Not even the growth direction of the neurites seems to be affected by this Ta_2O_5 structure

size. The growth is at first glance identical to that of the larger SiO_2 areas which agrees with observations in the literature [44]. However, in this work we only tried a very small spacing as a first test. More work on different designs (e.g. variations of SiO_2 linewidth and Ta_2O_5 spacing) would be necessary to find out up to which distance neurons are capable to span their surrounding in this system and whether a directed growth of the neurites is possible with this type of patterning.

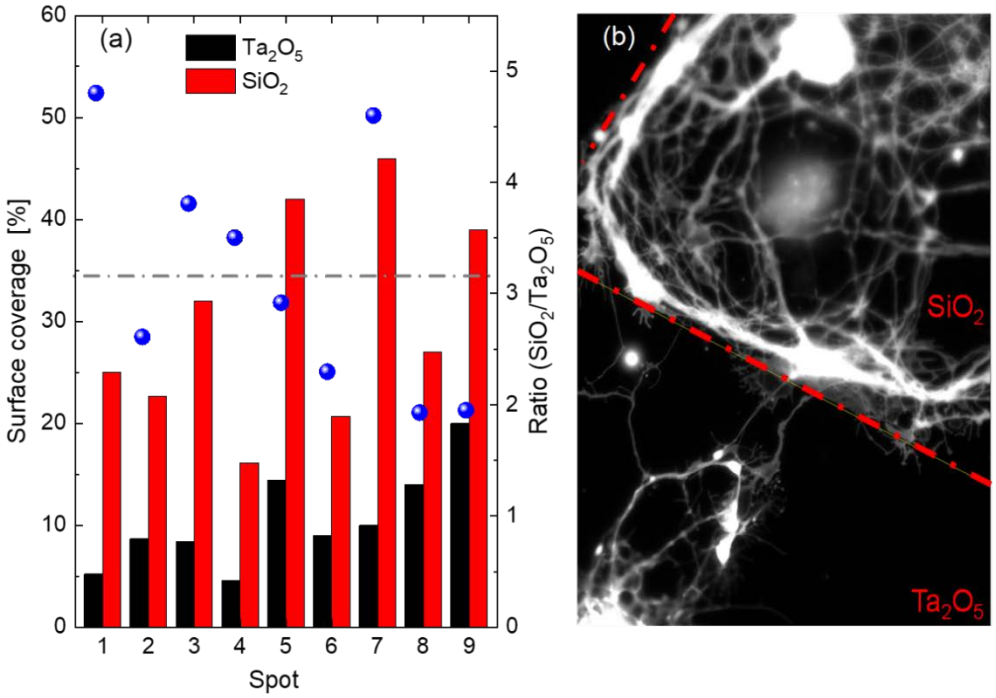

Figure 9. (a) Neurite and growth cone surface coverage for nine different spots (size 1.5×10^4 μm^2) on the patterned sample with similar areas of APTES-coated SiO_2 and Ta_2O_5. Red and black bars mark the respective surface coverage on SiO_2 and Ta_2O_5, the blue dots represent the ratio of the coverages of these two for the respective spots. (b) Typical example of a chosen area showing the neuronal morphology on SiO_2 versus Ta_2O_5.

In order to verify the different growth behaviors on SiO_2 and Ta_2O_5, we analyzed the amount of surface coverage with neurites and growth cones, which can be taken as a measure for the growth activity of the neurons. The amount of neurite and growth cone covered surface is obtained from fluorescence images. By converting the images into gray scale images with adequate contrast, the substrate turns black, soma and neurite bundles become white, and the neurites and their growth cones are gray (see Figure 9b). The amount of gray pixels can then be taken as a measure for the amount of neurites and their growth cones. Figure 9a shows the resulting percentage of the surface covered by dendrites and growth cones for different positions on the patterned substrate. The

positions are chosen arbitrarily at borders between SiO_2 and Ta_2O_5 and an area of 1.5×10^4 µm^2 is examined, which includes similar regions on SiO_2 and Ta_2O_5. Although the surface coverage varies for the different positions, it is always significantly higher for the SiO_2 area compared to the adjacent Ta_2O_5 area. For SiO_2 it ranges from ~15 % to 45 %, whereas it is 5 % to 20 % for Ta_2O_5. On average the coverage with dendrites and growth cones is approximately 3.2 times larger for SiO_2 compared to Ta_2O_5. Although this number is smaller than the cell density contrast on plain APTES-coated SiO_2 and Ta_2O_5 surfaces, it demonstrates that a preferential maturation of neurons on SiO_2 area (i.e. guided growth) is also present on patterned SiO_2-Ta_2O_5 surfaces.

CONCLUSIONS

In this work, we demonstrated that neuronal cell growth can be guided on a substrate by the use of different oxides, which are additionally functionalized with organic molecules. First, it is shown that the surface properties of the different oxides themselves are already quite different. For instance at physiological conditions the ζ potential ranges from approximately -62 mV (Ta_2O_5) to -49 mV (SiO_2) or -22 mV (Al_2O_3). Second, the oxide surface can be further modified by an additional functionalization with APTES layers. Only physisorbed layers (no chemical binding) can be achieved for some oxides (e.g. Ta_2O_5, TiO_2), whereas APTES SAMs form on other oxides (e.g. SiO_2, Al_2O_3). Not only does this affect the ζ potential (e.g. the ζ potential at physiological conditions increases from -49 mV to -27 mV on SiO_2, whereas it is unaltered for Ta_2O_5), it also affects the neuronal cell growth. The already high cell density on SiO_2 increases by the chemically bound APTES SAM, whereas the already low cell density on Ta_2O_5 is even further reduced by the physisorbed APTES layer. As a result we find a large difference in cell density (ratio of ~8) when comparing neuron cultures on SiO_2 and Ta_2O_5, both coated with APTES. Furthermore, neurons form the typical networks on SiO_2, whereas they tend to cluster to form neurospheres on Ta_2O_5. Finally, we utilized the large contrast in cell growth to achieve guided cell growth on reusable robust substrates. Using patterned Ta_2O_5 layers on SiO_2 substrates functionalized with APTES, the large difference in cell density and growth morphology is also visible for the patterned oxides. For example, on average ~3.2 times larger areas covered with neurites and growth cones are observed on SiO_2 areas compared to Ta_2O_5 areas. Furthermore, cell cultures and molecular layers can easily be removed and the cell experiment can be repeated after functionalization with the molecules. The general understanding and tailoring of inorganic surfaces via organic SAMs, demonstrated in this study for the combination of SiO_2, Ta_2O_5 and APTES, turned out to be a successful method to achieve guided cell growth and therefore might represent a beneficial step toward robust substrates with optimized interfaces for bioelectronics applications.

ASSOCIATED CONTENT

The following files are available free of charge.

XPS spectra, SEM image and XRD Bragg-Brentano pattern of ALD Ta_2O_5 specimen (Figure S1);diagram of the MLD setup (Figure S2); development of the ζ potential for SiO_2 and Ta_2O_5 after coating with APTES and cleaning for streaming current measurement (Figure S3); and schematic of the streaming current measurements (Figure S4). (PDF)

ACKNOWLEDGMENTS

The authors would like to thank Dr. Jürgen Moers, Rolf Kutzner, Matthias Geitner, Dr. Elmar Neumann, Stephany Bunte, Dr. Florian Lentz, Dr. Heinrich Hartmann, Dr. Uwe Breuer, Bettina Breuer (for neuronal isolation), the Helmholtz Nanoelectronic Facility (HNF) for productive cooperation, and Agnieszka Kurek and Harm Knoops from Oxford Instruments Plasma Technology for providing standard recipe parameters for the deposition of the different oxides. X. Yuan would like to thank the China Scholarship Council (CSC) for its financial support, grant number 201609370032.

REFERENCES:

(1) Zhang, L.; Webster, T. Nanotechnology and Nanomaterials: Promises for Improved Tissue Regeneration. *Nano Today* **2009**, 4, 66-80.

(2) Widge, A.; Jeffries-El, M; Cui, X; Lagenaur, C.; Matsuoka, Y. Self-assembled Monolayers of Polythiophene Conductive Polymers Improve Biocompatibility and Electrical Impedance of Neural Electrodes. *Biosens. Bioelectron.* **2007**, 22, 1723-1732.

(3) Markov, A.; Maybeck, V.; Wolf, N.; Mayer, D.; Offenhäusser, A.; Wördenweber, R. Engineering of Neuron Growth and Enhancing Cell-Chip Communication via Mixed SAMs. *ACS Appl. Mater. Interfaces* **2018**, 10, 18507-18514.

(4) Feinerman, O.; Rotem, A.; Moses, E. Reliable Neuronal Logic Devices from Patterned Hippocampal Cultures. *Nat. Phys.* **2008**, 4, 967-973.

(5) Wang, P.; Xu, G.; Qin, L.; Xu, Y.; Li, Y.; Li, R. Cell-based Biosensors and Its Application in Biomedicine. *Sens. Actuators, B.* **2005**, 108, 576-584.

(6) Roth, E.; Xu, T.; Das, M.; Gregory, C.; Hickmann, J.; Boland, T. Inkjet Printing for High-throughput Cell Patterning. *Biomaterials* **2004**, 17, 3707-3715.

(7) Xu, T.; Zhao, W.; Zhu, J.; Albanna, M.; Yoo, J.; Atala, A. Complex Heterogeneous Tissue Constructs Containing Multiple Cell Types Prepared by Inkjet Printing Technology. *Biomaterials* **2013**, 34, 130-139.

(8) Matsusaki, M.; Sakaue, K.; Kadowaki, K.; Akashi, M. Three-Dimensional Human Tissue Chips Fabricated by Rapid and Automatic Inkjet Cell Printing. *Adv. Healthcare Mater.* **2013**, 2, 534-539.

(9) Yamaguchi, S.; Ueno, A.; Akiyama, Y.; Morishima, K. Cell Patterning Through Inkjet Printing of

One Cell Per Droplet. *Biofabrication* **2012**, 4, 1-8.

(10) Tasoglu, S.; Demirci, U. Bioprinting for Stem Cell Research. *Trends Biotechnol.* **2013**, 31, 10-19.

(11) Staii, C.; Viesselmann, C.; Ballweg, J.; Shi, L.; Liu, G.; Williams, J.; Dent, E.; Coppersmith, S.; Eriksson, M. Positioning and Guidance of Neurons on Gold Surfaces by Directed Assembly of Proteins using Atomic Force Microscopy. *Biomaterials* **2009**, 30, 3397-3404.

(12) Kwiat, M.; Elnathan, R.; Pevzner, A.; Peretz, A.; Barak, B.; Peretz, H.; Ducobni, T.; Stein, D.; Mittelman, L.; Ashery, U.; Patolsky, F. Highly Ordered Large-Scale Neuronal Networks of Individual Cells-Toward Single Cell to 3D Nanowire Intracellular Interfaces. *ACS Appl. Mater. Interfaces* **2012**, 4, 3542-3549.

(13) Roach, P.; Parker, T.; Gadegaard, N.; Alexandr, M. Surface Strategies for Control of Neuronal Cell Adhesion: A review. *Surf. Sci. Rep.* **2010**, 65, 145-173.

(14) Hardelauf, H.; Waide, S.; Sisnaike, J.; Jacob, P.; Hausherr, V.; Schöbel, N.: Janasek, D.; Van Thriel, C.; West, J. Micropatterning Neuronal Networks. *Analyst* **2014**, 139, 3256-3264.

(15) Chang, H.; Kao, W.; You, Y.; Chu, Y.; Chu, K.; Chen, P.: Wu, C.; Lee, Y.; Shyue, J. Effect of Surface Potential on Epithelial Cell Adhesion, Proliferation and Morphology. *Colloid Surface B.* **2016**, 141, 179-186.

(16) Barry III, R.; Shepherd, R.; Hanson, J.; Nuzzo, R.; Wiltzius, P.; Lewis, J. Direct-Write Assembly of 3D Hydrogel Scaffolds for Guided Cell Growth. *Adv. Mater.* **2009**, 21, 2407-2410.

(17) Yu, T.; Shoichet, M. Guided Cell Adhesion and Outgrowth in Peptide-modified Channels for Neural Tissue Engineering. *Biomaterials* **2005**, 13, 1507-1514.

(18) Li, Y.; Xiao, Y.; Liu, C. The Horizon of Materiobiology: A Perspective on Material-Guided

Cell Behaviors and Tissue Engineering. *Chem. Rev.* **2017**, 117, 4376-4421.

(19) Schwaab, D.; Zentis, P.; Winter, S.; Meffert, S.; Offenhäusser, A.; Mayer, D. Generation of Protein Nanogradients by Microcontact Printing. *Jpn. J. Appl. Phys.* **2013**, 52, 191-195.

(20) Santhanam, V.; Andres, R. Microcontact Printing of Uniform Nanoparticle Arrays. *Nano Lett.* **2004**, 4, 41-44.

(21) Fricke, R.; Zentis, P.; Rajappa, L.; Hofmann, B.; Banzet, M.; Offenhäusser, A.; Meffert, S. Axon Guidance of Rat Cortical Neurons by Microcontact Printed Gradients. *Biomaterials.* **2011**, 32, 2070-2076.

(22) Fink, J.; Thery, M.; Azioune, A.; Dupont, R.; Chatelain, F.; Bornens, M.; Piel, M. Comparative Study and Improvement of Current Cell Micro-patterning Techniques. *Lab Chip.* **2007**, 7, 672-680.

(23) Guillotin, B.; Guillemot, F. Cell Patterning Technologies for Organotypic Tissue Fabrication. *Trends Biotechnol.* **2011**, 29, 183-190.

(24) Qin, D.; Xia, Y.; Whitesides, G. Soft Lithography for Micro- and Nanoscale Patterning. *Nat. Protoc.* **2010**, 491-502.

(25) Zheng, W.; Zhang, W.; Jiang, X. Precise Control of Cell Adhesion by Combination of Surface Chemistry and Soft Lithography. *Adv. Healthcare Mater.* **2013**, 2, 95-108.

(26) Arima, Y.; Iwata, H. Effect of Wettability and Surface Functional Groups on Protein Adsorption and Cell Adhesion Using Well-defined Mixed Self-assembled Monolayers. *Biomaterials* **2007**, 28, 3074-3082.

(27) Nam, Y.; Branch, D.; Wheeler, B. Epoxy-silane Linking of Biomolecules is Simple and Effective

for Patterning Neuronal Cultures. *Biosens. Bioelectron.* **2006**, 22, 589-597.

(28) Fang, Y.; Li, X.; Fang, Y. Organic Bioelectronics for Neural Interfaces. *J. Mater. Chem. C.* **2015**, 3, 6424-6430.

(29) Schvartzman, M.; Palma, M.; Sable, J.; Abramson, J.; Hu, X.; Sheetz, M.; Wind, S. Nanolithographic Control of the Spatial Organization of Cellular Adhesion Receptors at the Single-Molecule Level. *Nano Lett.* **2011**, 11, 1306-1312.

(30) Chang, W.; Sretavan, D. Novel High-Resolution Micropatterning for Neuron Culture Using

Polylysine Adsorption on a Cell Repellant, Plasma-Polymerized Background. *Langmuir* **2008**, 24, 13048-13057

(31) Joo, S.; Kang, K.; Nam, Y. In Vitroneurite Guidance Effects Induced by Polylysine Pinstripe Micropatterns with Polylysine Background. *J. Biomed. Mater. Res. A* **2015**, 103, 2731-2739.

(32) Veiseh, M.; Wickes, B.; Castner, D.; Zhang, M. Guided Cell Patterning on Gold-silicon Dioxide Substrates by Surface Molecular Engineering. *Biomaterials* **2004**, 25, 3315-3324.

(33) Lan, S.; Veiseh, M.; Zhang, M. Surface Modification of Silicon and Gold-patterned Silicon Surfaces for Improved Biocompatibility and Cell Patterning Selectivity. *Biosens. Bioelectron.* **2004**, 20, 1697-1708.

(34) Kim, Y.; Baek, N.; Han, Y.; Chung, M.; Jung, S. Enhancement of Neuronal Cell Adhesion by Covalent Binding of Poly-d-lysine. *J. Neurosci. Methods* **2011**, 202, 38-44.

(35) Murugan, R.; Molnar, P.; Rao, K.; Hickmann, J. Biomaterial Surface Patterning of Self Assembled Monolayers for Controlling Neuronal Cell Behavior. *Int J Biomed Eng Technol*. **2009**, 2, 104-134.

(36) Mrksich, M. A Surface Chemistry Approach to Studying Cell Adhesion. *Chem. Soc. Rev.* **2000**, 29, 267-273.

(37) Knoll, W. Handbook of Biofunctional Surfaces, *CRC Press* **2012**, 3-30.

(38) Li, P.; Greben, K.; Wördenweber, R.; Simon, U.; Offenhäusser, A.; Mayer, D. Tuning Neuron Adhesion and Neurite Guiding Using Functionalized AuNPs and Backfill Chemistry. *RSC Adv.***2015**, 5, 39252-39262.

(39) Imani, S.; Badv, M.; Shakeri, A.; Yousefi, H.; Yip, D.; Fine, C.; Didar, T. Micropatterned Biofunctional Lubricant-infused Surface Promote Selective Localized Cell Adhesion and Patterning. *Lab Chip*. **2019**, 19, 3228-3237.

(40) Yuan, X.; Wolf, N.; Mayer, D.; Offenhäusser, A.; Wördenweber, R. Vapor-Phase Deposition and Electronic Characterization of 3-Aminopropyltriethoxysilane Self-Assembled Monolayers on Silicon Dioxide. *Langmuir* **2019**, 35, 8183-8190.

(41) Markov, A.; Wolf, N.; Yuan, X.; Mayer, D.; Maybeck, V.; Offenhäusser, A.; Wördenweber, R. Controlled Engineering of Oxide Surfaces for Bioelectronics Applications Using Organic Mixed Monolayers. *ACS Appl. Mater. Interfaces* **2017**, 9, 29265-29272.

(42) Greben, K.; Li, P.; Mayer, D.; Offenhäusser, A.; Wördenweber, R. Immobilization and Surface Functionalization of Gold Nanoparticles Monitored via Streaming Current/potential Measurements. *J. Phys. Chem. B* **2015**, 119, 5988-5994.

(43) Hermanson, G. Fluorescent Probes. Bioconjugate Techniques (Third edition) **2013**, 395-463.

(44) Petrelli, A.; Marconi, E.; Salerno, M.; De Pietri Tonelli, D.; Berdondini, L.; Dante, S. Nano-volume Drop Patterning for Rapid on-chip Neuronal Connect-ability Assays. *Lab Chip*. **2013**, 13, 4419-4429.